ABSTRACT

COMPUTATIONAL STUDIES OF ELECTRONIC STRUCTURE
OF DOPED GRAPHENE

by
Yan Chu

In the literature, extensive studies have been performed to study the electronic properties of doped graphene. This is due to the potentially large number of applications of graphene in p-n junctions, transistors, photodiodes and lasers. By utilizing single heteroatom chemical doping method or electric field-induced method, one can introduce a band gap, ranging from 0.1eV to 0.5eV, in graphene. A tunable bandgap is highly desirable because it would allow significant flexibility in the design and optimization of such devices, particularly if it could be tuned by adjusting the doping configurations. Here, we demonstrate the realization of a widely tunable electronic bandgap in B and N co-doped graphene, of which the dopant concentration is from 6.25% to 75%. A recent study of the impact of co-doping on the band gap and bond length of graphene, from Pooja Rani Research Group in 2013, has inspired this research to further investigate the co-doping method. Materials Studio simulation tool, based on Density Functional Theory, has been utilized in this study. The simulations show that, with up to 75% concentration, a 2.99eV wide band gap is obtained. An ascending trend line (band gap as a function of dopant atoms) is also obtained from extensive simulation results. The results of this work, i.e., heteroatoms co-doping band gap control suggests novel nanoelectronics device applications based on graphene.

COMPUTATIONAL STUDIES OF ELECTRONIC STRUCTURE
OF DOPED GRAPHENE

by
Yan   Chu

Blank Page

BIOGRAPHICAL SKETCH

Author: Yan Chu

Degree: Master of Science

Date: May 2015

Undergraduate and Graduate Education:

- Master of Science in Materials Science and Engineering,
  New Jersey Institute of Technology, Newark, NJ, 2015

- Bachelor of Engineering in Metal Science,
  Shanghai University, Shanghai, P. R. China, 2010

Major: Materials Science and Engineering

ACKNOWLEDGMENTS

TABLE OF CONTENTS

TABLE OF CONTENTS
(Continued)

LIST OF TABLES

LIST OF FIGURES

CHAPTER 1

INTRODUCTION

1.1 Objectives

Due to their unique optical, electronic and mechanical properties, tremendous research has been conducted on 1D carbon nanotube and 2D graphene, leveraging advances in frontiers in science and technology. These nanomaterials, of which a single unit is in size between 1 and 100nm, have great potentials in the application of electronic devices, energy conversion, and hydrogen storage.

In this study, a materials modeling and simulation software, Materials Studio (MS), was used to calculate the 1D nanomaterial——graphene's electronic band structure, investigate the effect of chemical doping and explain the formation of band gap.

Materials Studio (MS) is a combination of totally 25 well-developed codes, including the well-known DMol3, CASTEP, and GUSSIAN, and a built-in materials modeling visualizer, which allows materials engineers and scientists a complete computational method to predict and understand the relationships of a material's atomic and molecular structure, properties and behavior. It is an extensive tool that can both conduct quantum scale and atomic scale ab initio calculations.

In this study, band structure investigation was extensively conducted as a function of dopant isomers and doping sites, by utilizing DMol3. All the simulation results largely agree with the literature. The ultimate objective of this study is to offer a basis for achieving band gap engineering, a controlled process of band gap opening and a basis that a graphene structure with a certain dopant configuration can be ultimately used in suitable electronic devices.

1.2 Methods

The DMol3 code, which was used in this study, is a validated Density Functional Theory (DFT) based computing code that can calculate electronic band structure accurately in carbon nanotube and graphene. All band structure calculations were conducted only after the total energy of the cell structures, which were drafted in Materials Studio Visualizer, reached the minimum. Through this process, the results can be mostly close to the empirical counterparts in the literature.

In terms of setting up the parameters for electronic options in DMol3, by referring to related publications and on-line help resources provided by MS, a set of comparatively accurate (quality) parameters were selected through the band structure calculations. The key parameters are Integration Accuracy, Self-Consistent Field (SCF) tolerance, K-points, Core Treatment and Cut-off Energy.

In terms of 2D crystal building in MS Visualizer, more than 20 Å distance along the Z direction, which is perpendicular to graphene sheet (X and Y directions), was set up to decrease interactions between the layers. The ultra-long distance can be viewed as an infinite vacuum environment imposed between graphene sheets in MS.

1.3 Significance

To the best of our knowledge, simulation tools such as COMSOL Multiphysics, MATLAB, Ansys etc. have been significantly adopted in the industry. Manufactures, engineers and scientists are benefiting significantly from simulation software, which is a time-saving and cost-saving approach.

By using MS, innovative material structures and properties are accelerated for better performance. Furthermore, MS enables users to have a reduction of up to 10 times in the number of experiments required to introduce a new synthesis.

The present study of electronic properties on chemically doped graphene, by utilizing MS, will provide a basis for nano-related research and innovations based on computing methods, and will serve as a good support for empirical studies in the future.

CHAPTER 2

RESEARCH BACKGROUND

2.1 Discovery of Graphene

Graphene had already been studied theoretically in 1947 by Wallace PR [1] as a text book example for calculations in solid state physics and was discovered realistically by the Geim group at the University of Manchester, UK, in 2004. Andre Geim and Konstantin Novoselov were awarded the Nobel Prize in Physics in 2010. Graphene is the name given to a single layer of sp^2-bonded carbon atoms arranged in a honeycomb structure, which is the first true 2D crystal. It is a thermodynamically stable two-dimensional material, in which the valence and conduction bands touch at the so called Dirac point in its intrinsic band structure and so is always referred as a semi-metal or zero-gap semiconductor. Since its successful fabrication in 2004 by micromechanical cleavage of graphite at the University of Manchester, UK, by the group of Geim, it has attracted great interest due to its fascinating properties and a large number of potential applications [2-6].

The density of graphene is $0.77mg/m^2$, with a breaking strength of 42N/m. A hypothetical steel film, with the same thickness as graphene, only has 0.0084-0.40 N/m. Graphene is almost transparent, with 2.3% absorption of light intensity. Graphene has unique physical properties such as massless relativistic Fermions that satisfy the Dirac equation, high electrical conductivity (even greater than silver) at room temperature, anomalous quantum Hall effect, finite conductivity even at zero charge carrier concentration and ballistic transport which originate from its hexagonal honeycomb lattice structure. The thermal conductivity of graphene has been measured to be approximately $5000Wm^{-1}K^{-1}$ (much larger than that of copper - $401Wm^{-1}K^{-1}$) [7-10]. All the above

properties make graphene a promising material for applications in nanoelectronics, sensors and optoelectronics. Especially, the linear dispersion curve at the Dirac point gives rise to exciting elementary electronic properties of graphene.

2.2 Electronic Properties of Graphene

The special character of the charge carriers is due to the intersection of the p/p* electronic bands occurring at the corners of its hexagonal Brillouin zone (Fig. 2.1). The P6/ MMM(in MS) hexagonal symmetry of the space group results in a band degeneracy at the high symmetry Dirac points (K and K') in the hexagonal Brillouin zone (BZ) leading to zero band gap. This absence of a tunable and sizable band gap in graphene poses limitations on its practical applications. So it is of crucial importance to find band gap opening methods to effectively tune the band gap of graphene for applications in nanoelectronics and optoelectronics [11, 12].
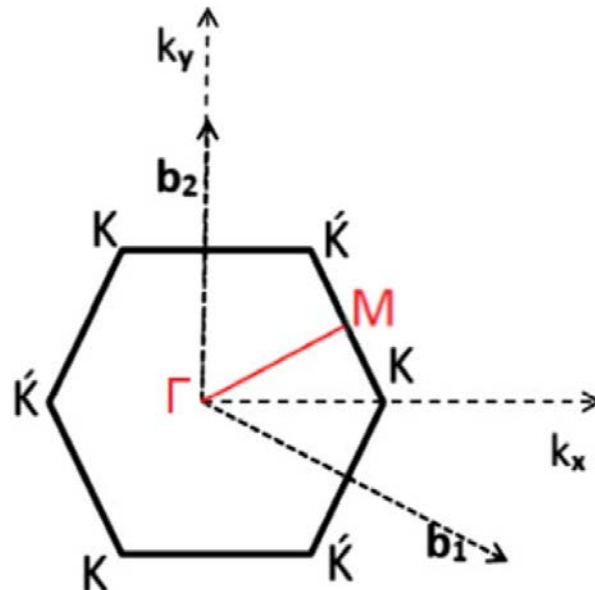
Figure 2.1 Brillouin zone sampling of graphene.

The electronic structure of graphene is rather different from usual three-dimensional or one-dimensional materials. Its Fermi surface is characterized by six double cones, as shown in Fig 2.2. In intrinsic (pristine) graphene, the Fermi level is situated at the connection points of these cones. Since the density of states of the material is zero at that point, the electrical conductivity of intrinsic graphene is quite low and is of the order of the conductance quantum $\sigma \sim 2e^2/h$. The Fermi level can, however, be changed by an electric field so that the material becomes either n-doped (with electrons) or p-doped (with holes) depending on the polarity of the applied field or changed by heteroatom doping (n-doped or p-doped). Graphene can also be doped by functionalization, for example, oxidized or hydrogenated on the surface [12].
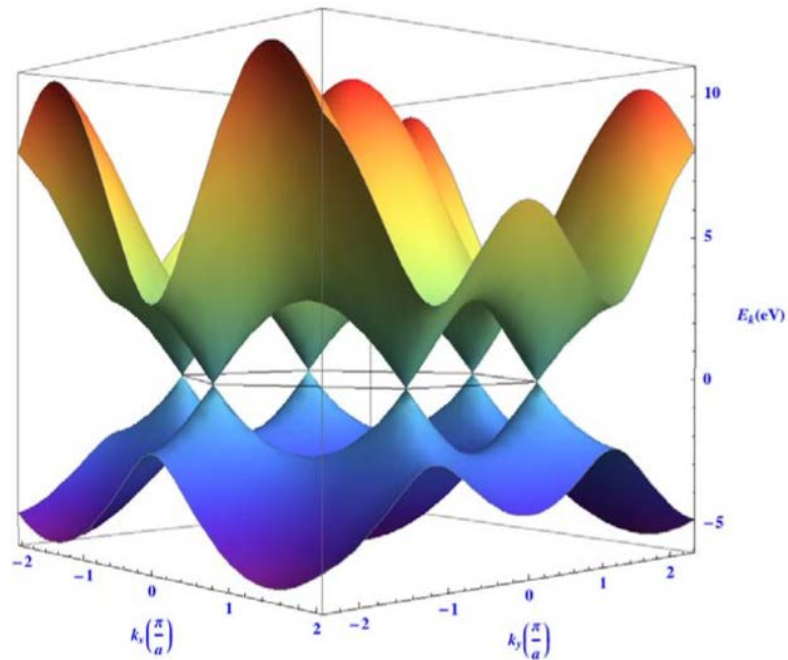
Figure 2.2 Fermi surface of graphene.

2.3 Literature Review of Band Gap Opening

Methods

Graphene is a novel semimetal (or zero band gap semiconductor) with high carrier mobility, high optical transparency and high tensile strength as stated above. However, for electronic device applications, the carrier concentration of the carbon layer needs to be adjusted by shifting the Fermi level of graphene's unique crossed band gap at the Dirac point. The devices made from the zero-bandgap graphene are difficult to switch off, losing the advantage of the low static power consumption of the complementary metal oxide semiconductor (CMOS) technology. From a theoretical approach, there are various possibilities to introduce band gap in graphene. For example, oxidation of mono-vacancies in graphene [13], graphene/boron nitride heterobilayers [14], F-intercalated graphene on SiC substrate [15, 16], and substitutional carbon doping of boron nitride nanosheets, nanoribbons, and nanotubes have been reported [17].

Band gap opening methods, based on graphene, can be briefly categorized by six ways in terms of layer impact, chemically-induced and electric field-induced, providing basic clues for in-depth investigation of band gap opening behavior:

1. Heteroatom substitutional doping, such as boron (B), nitrogen (N), aluminum (Al), phosphorous (P) etc. [18].

2. Defect impact, e.g., holes (vacancies) patterning on graphene sheet (named graphene nanomesh) [19]; strain-induced defect, i.e. folding of graphene sheet [20].

3. Limit to 1D, graphene nanoribbon, with edge effect of zigzag or armchair [21].

4. Substrate-induced, e.g. SiC substrate [22], h-BN substrate [23].

5. Functionalization, covalent and non-covalent approaches [24].

6. Impact of layers:

   a) AB stack bilayer and multi even layer: electric field-induced and chemically-conjugated [25, 26].

   b) AA stack bilayer and multi even layers [27].

   c) ABA and ABC stack trilayer and multi odd layers [28].

2.4 Hetero Atom Doping of Graphene

2.4.1 Overview of Available Dopants

Hetero atom doping is the most feasible method to control the semiconducting properties and a widely used technique to modulate the electronic properties in graphene. The B and N atoms are the natural popular candidates for subsitutional doping in graphene because of their atomic size similar to that of C atom and their hole acceptor and electron donor characteristics for substitutional B- and N-doping, respectively. It has been shown that doping with B or N individually is an efficient method to introduce a shifting below or above the Fermi level (Fig 2.3) [29, 30].

Since 2010, several results have been reported on the effects of B/N co-doping. As compared to B–B or N–N bond lengths, B–N bond length is comparable to C–C bond length, which makes the combination of B–N a better choice to replace a C–C bond without causing much alteration to the 2-D lattice. The introduction of BN in graphene breaks the symmetry of graphene unit cell, which can result in the opening of a band gap in graphene and can be exploited for band gap-related applications.

Yu's group studied the effect of N/B doping on the electronic properties for a zero-dimensional zigzag-edged triangular structures. Their calculations showed that the triangular graphene with N/B doped in the major sub-lattice has a larger energy gap, and the electronic properties depend on the doping position [31]. It has been pointed out by Deng's group that, in case of BN co-doping, the gap is introduced at the Fermi level due to the combination of pull–push of boron and nitrogen [32]. Fan's group concluded that nano-domains of various geometrical shapes and sizes (h-BN sheet) can significantly change the electronic and magnetic properties of graphene [33]. Rani's group investigated isomers formed by choosing different doping sites and found that these sites differ significantly in relative stability and band gap introduced at the Dirac point [34]. Ci's group reported the synthesis and characterization of large-area atomic layers of h-BNC material, consisting of hybridized, randomly distributed domains of h-BN and C phases with compositions ranging from pure BN to pure graphene [35]. Inspired by these studies, our work of comparison of various isomers of B–C–N structure ranging from 6.25% to 75% and impact of layers on the B-N-C structure will be discussed in Chapters 4 and 5.

Utilizing computational simulation tools, apart from B/N atom, we can now investigate the band gap behavior with more possible dopants. Wei's group studied the effects of the interaction between the substitutional Si atoms doped in graphene and found that the band structure of graphene can be remarkably modulated by different Si doping configurations, leading to shift in Dirac point and even band-gap opening [36]. Denis's research group studied Al, Si, P and S doped graphene (monolayer and bilayer), stabilities of the structure and calculated the band gap with 3 at.% [37]. More heteroatoms are being explored. In the literature, researchers are investigating the stability of these heteroatoms doped into the

graphene sheet. However, due to their significant size mismatch with C atoms, the band gap behavior, as function of the doping concentration of these atoms and doping sites, need to be studied furthermore in the near future.
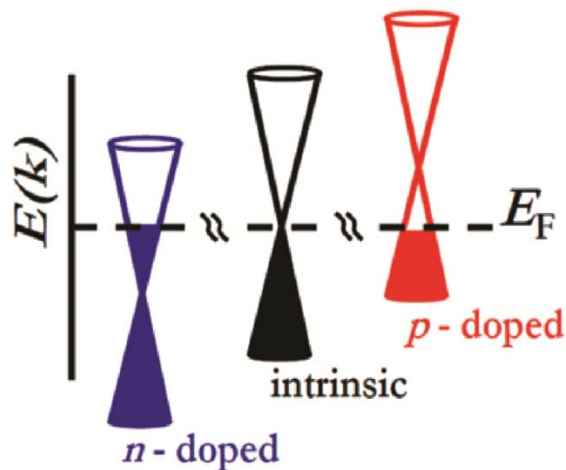
Figure 2.3 Sketch of pristine and doped graphene band structure.

2.4.2 Literature Review of Experimental Studies

The current progress in synthesis and doping methods of graphene and related materials and the corresponding band gap values are summarized in Table 2.1. The heteroatom doping methods and their typical effects on the physical properties of graphene are also included in the table. Diverse novel properties can be derived by chemical doping. From Table 2.1, we can see that the maximum band gap value we can get from empirical approach is 0.54ev resulting from B doping. It is realistic and practical that we can get a true band gap from chemical doping process. However, this kind of low level doping will not provide a promising material for tunable band gap for applications in nanoelectronics.

Table 2.1 Summary of Graphene Properties by Heteroatom Doping

Modification method	Mobility [$cm^2 V^{-1} s^{-1}$]	Conductivity [S/cm]	Work function [eV]	Band gap [eV]
Nitrogen doping	5–450 [graphene]	8333[a] [GO film]	3.98 [1% N_q –graphene]	Opened (value not mentioned)
	(value not mentioned)	(value not mentioned)	4.83 [1% N_p –graphene]	**0-0.2 (0-2.9%N-graphne)**
	(value not mentioned)	(value not mentioned)	4.92 [1% N_n -graphene]	(value not mentioned)
Boron doping	500–800 [graphene]	200–1000 [2%B-CNT]	1.7 lower than pristine CNT	**0-0.54 [0–13.85% B-graphene]**
Phosphorus doping	556 [graphene]	(value not mentioned)	(value not mentioned)	**0.3–0.4 [0.5% P-graphene]**
Sulfur doping	90 [2 % S-graphene]	4414[a] [graphene]	(value not mentioned)	**0.1–0.2 [0.5% S-graphene]**

Source: Uday Narayan Maiti , et. Al (2014) Chemically Modified/ Doped Carbon Nanotubes & Graphene for Optimized Nanostructures & Nanodevices. Advanced Materials 26: 40-67.

CHAPTER 3

BASICS OF DENSITY FUNCTIONAL THEORY

Using Materials Studio, researchers in many industries are designing and fabricating better performing materials of all types, including pharmaceuticals, catalysts, polymers and composites, metals and alloys, batteries and fuel cells, and more.

Materials Studio includes a graphical user environment—Materials Studio Visualizer— in which researchers can construct, manipulate and view models of molecules, crystalline materials, surfaces, polymers, and mesoscale structures. Materials Studio Visualizer is complemented by a complete set of solution methods including quantum, atomistic (or "classical"), mesoscale, and statistical approaches that enable scientists to evaluate materials at various particle sizes and time scales. It also includes tools for evaluating the crystal structure and crystal growth.

The following section describes an introduction to Dmol3 code——Density Functional Theory (MS) that we use in this thesis to study the electronic properties of graphene.

3.1 Introduction to Density Functional Theory

Density functional theory begins with a theorem by Hohenberg and Kohn (1964), later generalized by Levy (1979), which states that all ground-state properties are functionals of the charge density ρ. Specifically, the total energy, E_t, may be written as:

$$E_t[\rho] = T[\rho] + U[\rho] + E_{XC}[\rho]$$

$$(3.1)$$

where, $T[\rho]$ is the kinetic energy of a system of non-interacting particles of density ρ; U $[\rho]$ is the classical electrostatic energy due to Columbic interactions; $E_{xc}[\rho]$ includes all many-body contributions to the total energy, in particular, the exchange and correlation energies.

Eq. 3.1 is written to emphasize the explicit dependence of these quantities on ρ (in subsequent equations, this dependence is not always indicated).

The charge density is constructed from a wave function Ψ. As in other molecular orbital methods (Roothaan, 1951; Slater, 1972; Dewar, 1983), the wave function is taken to be an anti-symmetrized product (Slater determinant) of one-particle functions, in this case molecular orbitals (MOs),

$$\psi = \frac{1}{\sqrt{n!}}(n)|\phi_1(1)\phi_2(2) \dots \phi_n(n)|$$

(3.2)

When the molecular orbitals are orthonormal,

$$\langle \phi_i | \phi_j \rangle = \delta_{ij}$$

(3.3)

The charge density is given by the simple sum,

$$\rho(\mathbf{r}) = \sum_i |\phi_i(\mathbf{r})|^2$$

(3.4)

where the sum is over all occupied MOs, ϕ_i. The density obtained from this expression is also known as the *charge density*. The MOs may be occupied by spin-up (alpha) or spin-down (beta) electrons. Using the same ϕ_i

for both alpha and beta electrons is known as a *spin-restricted* calculation; using different ϕ_i for alpha and beta electrons results in a *spin-unrestricted* or *spin-polarized* calculation. In the unrestricted case, it is possible to form two different charge densities: one for alpha MOs and one for beta MOs. Their sum gives the total charge density and their difference gives the *spin density*, the amount of excess alpha over beta spin. This is analogous to restricted and unrestricted Hartree-Fock calculations (Pople and Nesbet, 1954).

3.2 Total Energy Components

From the wave functions and the charge density (Eq. 4), the energy components can be written (in atomic units) as:

$$T = \left\langle \sum_i^n \phi_i \left| \frac{-\nabla^2}{2} \right| \phi_i \right\rangle$$

(3.5)

$$U = \int V_N(\mathbf{r})\rho(\mathbf{r})d\mathbf{r} + \frac{1}{2}\int \frac{\rho(\mathbf{r}_1)\rho(\mathbf{r}_2)}{|\mathbf{r}_1 - \mathbf{r}_2|}d\mathbf{r}_1 d\mathbf{r}_2 + V_{NN}$$

(3.6)

- The first term represents the electron-nucleus attraction.

- The second term represents the electron- repulsion.

- The final term, V_{NN}, represents the nucleus- repulsion.

3.3 Approximating the Exchange-Correlation Energy

The final term in Eq. 3.1, the exchange-correlation energy, requires some approximation for this method to be computationally tractable. A simple and good approximation is the local density approximation (LDA), which is based on the known exchange-correlation energy of the uniform electron gas (Hedin and Lundqvist, 1971; Ceperley and Alder, 1980; Lundqvist and March, 1983). Analytical representations have been made by several researchers (Hedin and Lundqvist, 1971; Ceperley and Alder, 1980; von Barth and Hedin, 1972; Vosko et al., 1980; Perdew and Wang, 1992). The local density approximation assumes that the charge density varies slowly on an atomic scale (i.e., each region of a molecule actually looks like a uniform electron gas). The total exchange-correlation energy can be obtained by integrating the uniform electron gas result:

$$E_{XC}[\rho] \cong \int \rho(\mathbf{r}) \varepsilon_{XC}[\rho(\mathbf{r})] \, d\mathbf{r}$$

(3.7)

where, $\varepsilon_{xc}[\rho]$ is the exchange-correlation energy per particle in a uniform electron gas and ρ is the number of particles.

3.4 Common Spin-density Functionals

The simplest form of the exchange-correlation potential is the form derived by Slater (1951), which simply uses $\varepsilon_{xc}[\rho] = \rho^{1/3}$. In this approximation, the correlation is not included. More sophisticated approximations use the forms derived by Vosko, Wilk, and Nusair (1980), denoted as VWN, Von Barth and Hedin (1972) (BH), Janak, Morruzi, and Williams (1975) (JMW), and Perdew and Wang (1992) (PW).

3.5 Density Gradient Expansion

The next step in improving the local density (LDA) model is to take into account the inhomogeneity of the electron gas which naturally occurs in any molecular system. This can be accomplished by a density gradient expansion, sometimes referred to as the non-local spin-density approximation (NLSD). Over the past few years, it has been well documented that the gradient-corrected exchange-correlation energy, $E_{xc}[\rho, d(\rho)/dr]$, is necessary to study the thermochemistry of molecular processes (see reviews by: Ziegler, 1991; Labanowski and Andzelm, 1991; Politzer and Seminario, 1995).

Commonly used NLSD functionals include the Perdew and Wang (PW) generalized gradient approximation for the correlation functional, the Becke (B) gradient-corrected exchange functional, and the gradient-corrected correlation functional of Lee, Yang, and Parr (LYP).

3.6 The Total Energy Expression

The total energy can now be written as:

$$E_t[\rho] = \sum_i \left\langle \phi_i \left| \frac{-\nabla^2}{2} \right| \phi_i \right\rangle + \left\langle \phi_i \left| \frac{-\nabla^2}{2} \right| \phi_i \right\rangle + \left\langle \rho(\mathbf{r_1}) \left[\varepsilon_{XC}[\rho(\mathbf{r_1})] + \frac{V_g(\mathbf{r_1})}{2} - V_N \right] \right\rangle + V_{NN}$$

(3.8)

3.7 Kohn-Sham Equations

In order to determine the actual energy, variations in E_t must be optimized with respect to variations in ρ, subject to the orthonormality constraints in Eq. 3.2 (Kohn and Sham, 1965). This process leads to a set of coupled equations first proposed by Kohn and Sham (1965):

$$\left\{ \frac{-\nabla^2}{2} - V_n + V_e + \mu_{XC}[\rho] \right\} \phi_i = \varepsilon_i \phi_i$$

(3.9)

The term, μ_{xc}, is the exchange-correlation potential, which results from differentiating E_{xc}. For the local spin-density approximation, the potential μ_{xc} is:

$$\mu_{XC} = \frac{\delta}{\delta\rho}(\rho\varepsilon_{XC})$$

(3.10)

Use of the eigenvalues of Eq. 3.9 leads to a reformulation of the energy expression:

$$E_t = \sum_i \varepsilon_i + \left\langle \rho(\mathbf{r}_1) \left[\varepsilon_{XC}[\rho] - \mu_{XC}[\rho] + \frac{V_e(\mathbf{r}_1)}{2} \right] \right\rangle + V_{NN}$$

(3.11)

3.8 Convenience of Expanding MOs in Terms of Basic Functions

In practice, it is convenient to expand the MOs in terms of atomic orbitals (AOs):

$$\phi_i = \sum_\mu C_{i\mu} \chi_\mu$$

(3.12)

The atomic orbitals, χ_μ, are called the atomic basis functions and the $C_{i\mu}$ are the MO expansion coefficients. Several choices are possible for the basis set, including Gaussian functions (Andzelm et al., 1989), Slater functions (Versluis and Ziegler, 1988), plane waves (Ashcroft and Mermin, 1976; Payne et al., 1992) and numerical orbitals.

Unlike the MOs, the AOs are not necessarily orthonormal. This leads to a reformulation in the form:

$$HC = \varepsilon SC \tag{3.13}$$

where:

$$H_{\mu\nu} = \left\langle \chi_\mu(\mathbf{r}_1) \left| \frac{-\nabla^2}{2} - V_N + V_e + \mu_{XC}\rho(\mathbf{r}_1) \right| \chi_\nu(\mathbf{r}_1) \right\rangle \tag{3.14}$$

and:

$$S_{\mu\nu} = \left\langle \chi_\mu(\mathbf{r}_1) \middle| \chi_\nu(\mathbf{r}_1) \right\rangle \tag{3.15}$$

3.9 LDA+U

Approximations of the DFT, described above, have proved to be very successful for the vast majority of compounds. However, they leave a class of so called "strongly correlated" systems beyond their consideration. These systems are usually described by the simplified

but true many body Hamiltonians, which are valid under different circumstances, but cannot efficiently be constructed *ab initio*.

The power of local density approximations (LDA) is very attractive and can be refined by considering a one-particle density matrix, n(s,r,s',r'), as a basic variable instead of spin density n(s,r). However, generalization of LDA faces a certain challenge: there are no exactly solvable problems which can be used to parameterize the generalized exchange-correlation energy. So models must be used.

One of the most successful models to describe correlated electrons in solids is the Hubbard model, on which the LDA+U extension of LDA is based. To construct an appropriate functional, the LDA+U approach subdivides charge density into two subsystems: delocalized and localized. The former remains described by its charge-density, while for the latter a site diagonal charge density matrix is introduced (Eq. 3.16).

$$n_{\mu\nu} = \langle \chi_\mu(\mathbf{r}) | n(\mathbf{r},\mathbf{r}') | \chi_\nu(\mathbf{r}') \rangle$$

(3.16)

In accordance with multiband Hubbard model, the effective LDA+U energy functional is written as:

$$E_{LDA+U} = E_{LDA} + E_{HF}(n_{\mu\nu}) - E_{dc}[n]$$

(3.17)

where, E_{LDA} denotes standard LDA energy functional. E_{HF} is Hartree-Fock like functional and E_{dc} is the double counting term, already taken into account in E_{LDA}.

U_{1324} are assumed to be renormalized Coulomb integrals and are virtually the only parameters entering the model.

$$E_{HF}(n_{\mu v}) = \frac{1}{2}\sum (U_{1324} - U_{1342})\, n_{12} n_{34}$$

(3.18)

A variational approach to minimizing the energy functional leads to the Kohn-Sham equations but with additional non-local potential:

$$V(\mathbf{r},\mathbf{r'}) = \sum_{34} \chi_1(\mathbf{r})\,(U_{1324} - U_{1342})\, n_{12} n_{34} \chi_2(\mathbf{r'})$$

(3.19)

which is to be calculated for each step of the self consistent field procedure.

3.10 SCF Procedure

Because H depends on C, Eq. 3.13 must be solved by an iterative technique. This can be done using the following procedure:

1. Choose an initial set of $C_{i\mu}$.

2. Construct an initial set of MOs ϕ_i.

3. Construct ρ via Eq. DFT-4.

4. Using ρ, construct V_e and μ_{xc}.

5. Construct $H_{\mu\nu}$.

6. Solve Eq. DFT-14 for a new set of $C_{i\mu}$.

7. Construct a new ϕ_i and a new ρ.

8. If $\rho_{new} = \rho_{old}$, evaluate E_t via Eq. DFT-12 and stop.

9. If $\rho_{new} \neq \rho_{old}$, return to Step 4.

For an organic molecule, about ten iterations are typically required to obtain convergence at $|\rho_{new} - \rho_{old}| < 10^{-6}$.

For metallic systems, many more iterations are frequently required.

3.11 Numerical Integration

Evaluation of the integrals in Eq. 3.14 must be accomplished by a 3D numerical integration procedure, due to the representation of the exchange-correlation potential. The matrix elements need to be approximated by the finite sums:

$$H_\mu \cong \sum_i \chi_\mu(\mathbf{r}_i) H_{eff}(\mathbf{r}_i) \chi_\nu(\mathbf{r}_i) w(\mathbf{r}_i)$$

(3.20)

3.12 Periodic Boundary Conditions

The discussion so far has been completely general with regard to the type of systems that can be studied with DFT. Molecules, clusters, or periodic solids are treated equally in this formalism. This section addresses some issues that specifically apply to infinite periodic systems. In the sections that follow, it is assumed that the system is periodic in three dimensions.

Consider a crystal with lattice vectors $\mathbf{a}_i$, i = 1, 2, 3. For example, in a simple cubic cell, the vectors could be $\mathbf{a}_1 = (1, 0, 0)$; $\mathbf{a}_2 = (0, 1, 0)$; and $\mathbf{a}_3 = (0, 0, 1)$. The basic functions must have the translational symmetry of the crystal, so $\chi_\mu(\mathbf{r}) = \chi_\mu(\mathbf{r} + \mathbf{R})$, where $\mathbf{r}$ is any point in the crystal and $\mathbf{R} = n_1\mathbf{a}_1 + n_2\mathbf{a}_2 + n_3\mathbf{a}_3$, with the n all being integers.

To meet this requirement, a set of plane waves with the periodicity of the lattice is generally introduced and the periodic basis is taken as $\psi(\mathbf{k},\mathbf{r}) = e^{i\mathbf{k}.\mathbf{R}}\chi(\mathbf{r})$.

There are, in principle, an infinite number of vectors $\mathbf{k}$ and $\mathbf{R}$ needed to describe the space exactly. In practice, the number of plane waves is determined by the cutoff kinetic energy which is chosen to represent physically relevant spatial harmonics of wave functions. The vectors $\mathbf{k}$ are called *k-points*, and are needed to describe the band structure correctly. In practice, only a few k-points (of the order of $1-10^2$) are needed.

3.13 Predicting Chemical Structure

The ability to evaluate the derivative of the total energy with respect to geometric changes is critical for the study of chemical systems. Without the first derivatives, a laborious point-by-point procedure is required, which is taxing to both computer and human resources. The availability of analytic energy derivatives for Hartree-Fock (Pulay, 1969),

CI (Brooks et al., 1980), and MBPT (Pople et al., 1979) theories (to name just a few) has made these remarkably successful methods for predicting chemical structures.

DFT offers an even more straightforward formalism for evaluating energy gradients, and thus it became the method of choice for structural studies of molecules and solids alike.

Future applications, suggested for DFT, include:

1. Design of hydrogen storage and designing new storage materials.

2. Design of molecular motors (for small systems that have functions of vehicles).

3. Design software and code development to facilitate computers do the simulation.

4. Aid in the design of new materials with novel properties.

CHAPTER 4

SIMULATION PROCESS

4.1 Modeling Details

The unit cell of graphene is 2-atom structure with 1.42nm in between and the bonds are periodic at an angle of 120° with respect to each other. From a macro point of view, it is a sheet of 2D hexagonal mesh [5, 37]. After sketching the graphene unit, the Brillouin zone path is built manually, as shown in Figure 4.1.
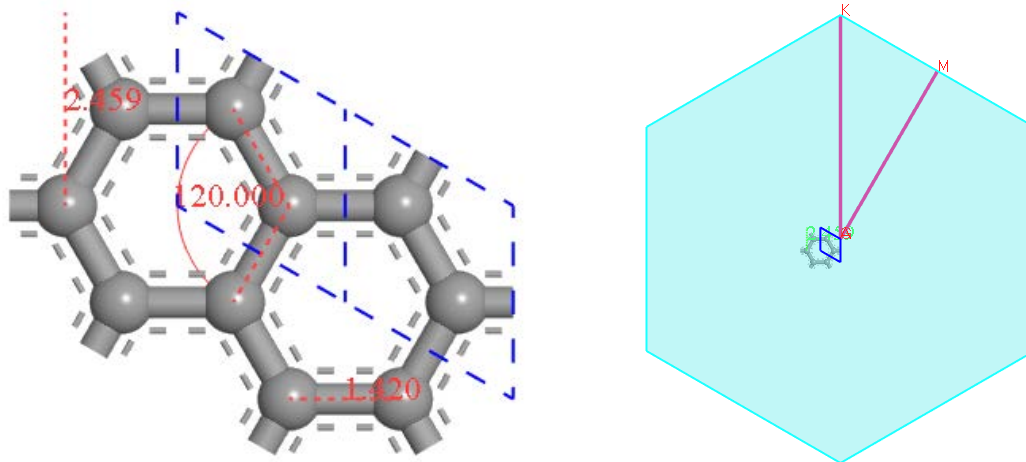

Figure 4.1 Sketching of graphene structure and Brillouin zone path.

The band structure and density of states of the unit cell are shown in Figure 4.2. The objective of this calculation, for pristine graphene, is to compare with the nitrogen-doped graphene.

(a)Band Structure   (b)Density of States
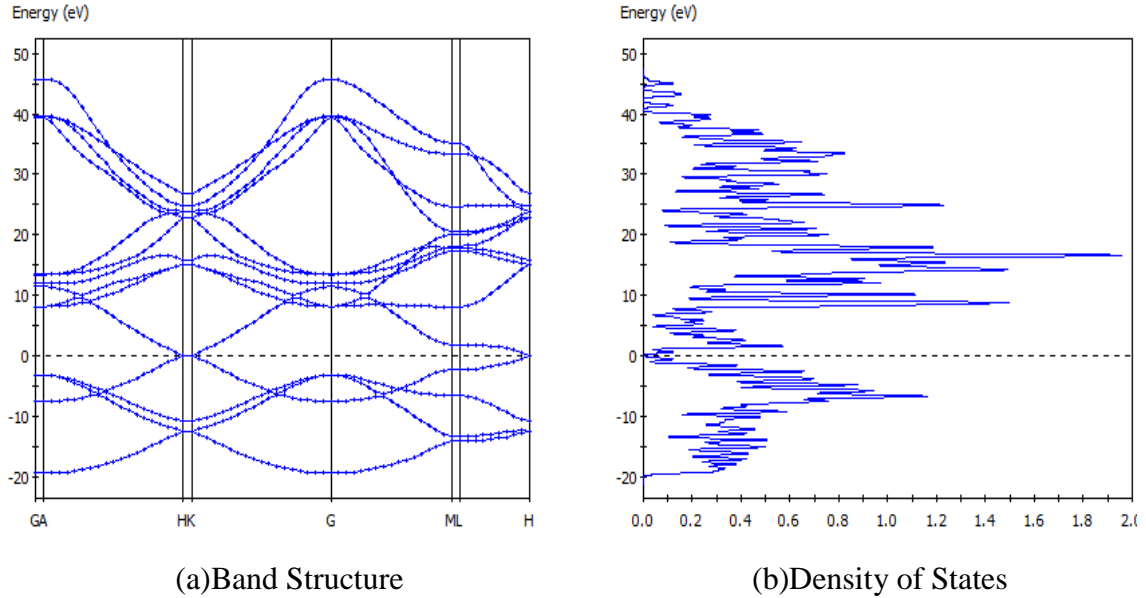
Figure 4.2 (a) Band Structure and (b) Density of States.

In order to realize the effect of nitrogen doping, we have two ways to construct a model. One way is that, firstly, we build a large pristine graphene sheet, composed of ~100 carbon atoms. The carbon atoms are then replaced with nitrogen atoms. The amount of replacement is gradual, from 1, 2, 3 … to 15 atoms. For each replacement, a band gap resulting from that specific replacement can be calculated. This method can be understood by fixing the periodicity of graphene dimensions while increasing the dopant percentage.

The other approach is a reverse method in which, firstly, we build an 8-atom graphene cell and replace only one carbon atom with nitrogen atom. We call this structure base cell. Then, gradually, we build more pristine graphene cells periodically on to the base cell. The more the number of pristine cells added, the less is the nitrogen dopant concentration. This method can be easily understood by fixing the dopant concentration while increasing the graphene dimension, as shown in Figure 4.3.

25

| (a)Unit | (b)8-atom | (c)8-atom | (d)18-atom | (e)98-atom |
| Cell | Cell | Base Cell | | |
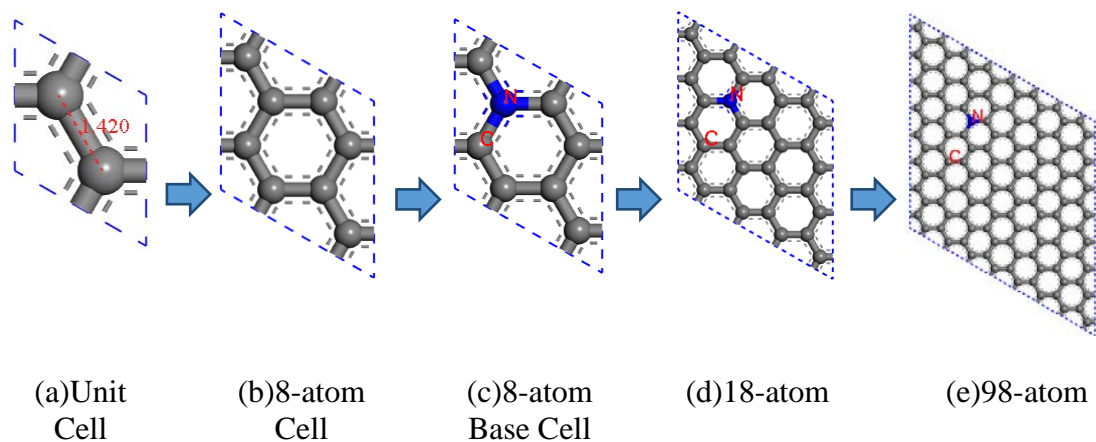
Figure 4.3 Modeling of nitrogen doped graphene.

Furthermore, from the literature [38], we know that nitrogen forms three types of bonding with carbon; these are graphitic nitrogen, pyridine nitrogen and pyrrole nitrogen.
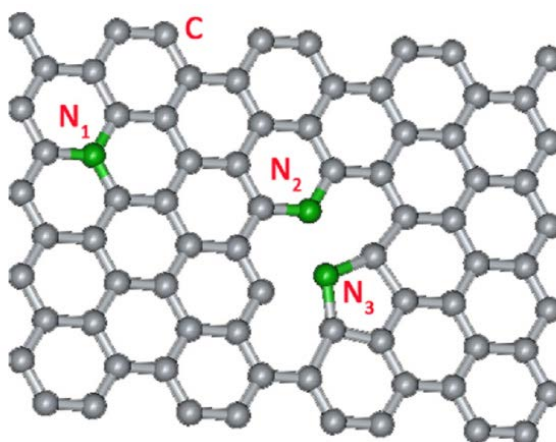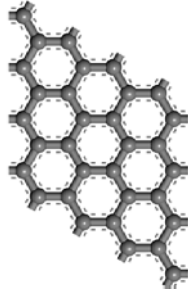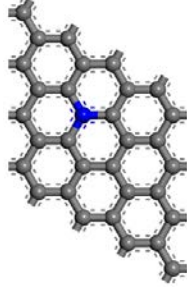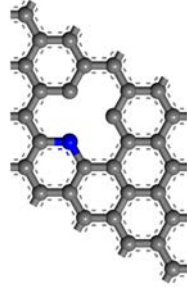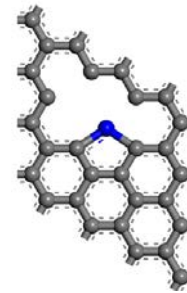
Figure 4.4 Molecular models of N1 graphitic nitrogen, N2 pyridine nitrogen and N3 pyrrole nitrogen.

N2 (Pyridine) and N3 (Pyrrole) structures have been modeled accordingly and the total energy has been calculated. From the table listed below, the total energy of N1, N2 and N3 is respectively -1225.899229, -1187.866883 and -1150.020095Ha, decreasing slightly

progressively with reduced amount of super cell atoms. The total energy is composed of sum of atomic energies - kinetic, electrostatic, exchange-correlation and spin polarization.

Table 4.1 Total Energy of Various Nitrogen Doped Graphene Structures (Nitrogen atom is indicated by blue color, and carbon atoms are grey.)

	Pristine	N1(Graphitic)	N2(Pyridine)	N3(Pyrrole)
Supercell Models (Post Geometry Optimization)				
Atom Amount	32	32	31	30
Total Energy (Ha)	-1209.364815	-1225.899229	-1187.866883	-1150.02009
Binding Energy (Ha)	-10.4147074	-10.2822889	-9.7171336	-9.3375363

By sketching the structures and optimizing the geometry, these models are ready to be used to conduct further simulation of band gap and compare with experimental data from the literature.

4.2 Parameter Setting

The K-point set affects the energy calculation of the structure along with the band structure. Total energy calculation will be different in accordance with the different model structure.

Thus the K –point setting is a vital factor in the entire simulation process. Several K -point set from coarse quality to fine were considered, from 4x4x1, 6x6x1… to 14x14x1. Energy for each set was calculated. For example, in terms of a unit cell of graphene, 2-atom cell, and fluctuating energy is as follows: 6x6x1 and 12x12x1 set has the lowest energy and accordingly, going through the output data sheet, the simulation program indicates that this is a semi-metal.

The DFT code used in this study is Dmol3, local functional PWC, spin unrestricted. More details can be found in Table 4.2
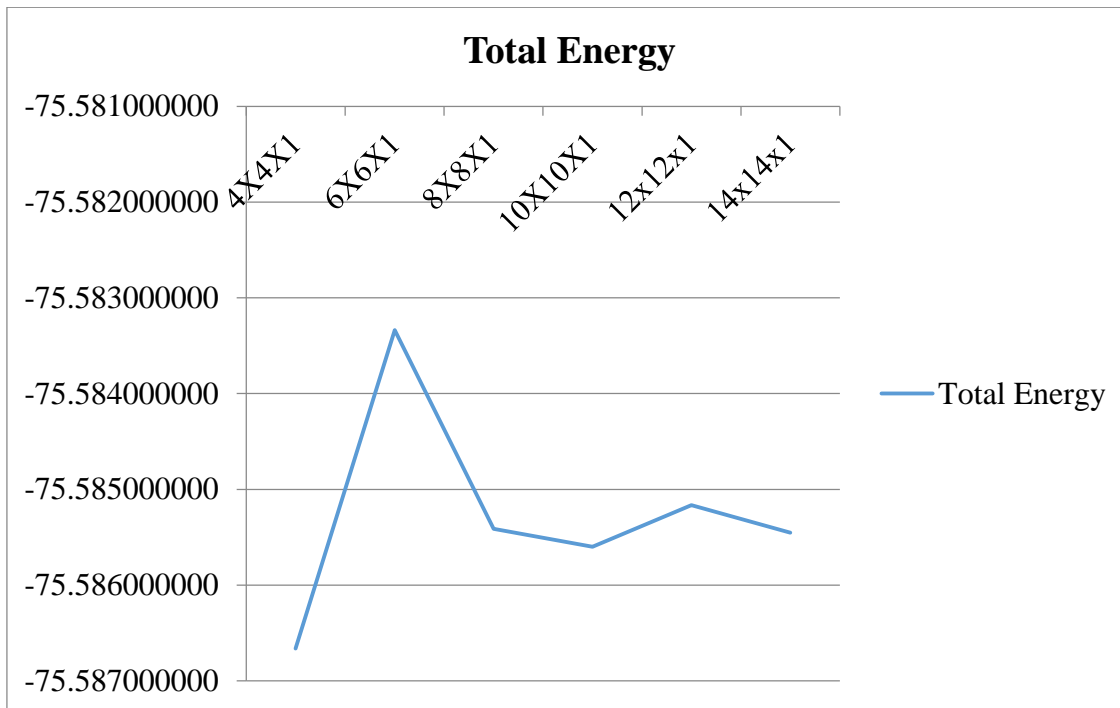
Figure 4.5 Graph of total energy as a function of K-point set for unit cell of graphene (The unit of total energy is Ha).

Table 4.2 Parameter Setting for Calculation of Band Structure and Density of States

DFT Code	Dmol3
K-point Set	From 5x5x1, 6x6x1 … to 14x14x1
Pseudopotential	None
Functional	GGA PBE
Energy Cut Off	Global, fine quality
Spin	Unrestricted
Symmetry	Yes
SCF Tolerance	1.0e-5
Max. SCF Cycles	50
Energy Bands	20

All the band structure results in Chapter 5 are sketched within the same scale from +4ev to -4ev and the Brillouin zone path was sampled in the order of K-G-M-K-G for efficient comparison.

CHAPTER 5

RESULTS AND DISCUSSION

The redistribution of surface charge which breaks the local symmetry of graphene is the main reason for band gap opening of graphene on B/N codoping, which leads to the separation of the valence band and conduction band of graphene at the Dirac point. Since B doping leads to band gap opening above the Fermi level and N doping, below the Fermi level, the counterbalance of both creates a gap at the Fermi level. In addition, the Coulomb dipole from B/N bonds may also be important to the breaking of symmetry of graphene structure and thus to the band gap opening. Single atom type doping and co-doping are both studied and compared. Furthermore, the doping sites, i.e. configuration of doping structure are also discussed. All the results are conducted under code Dmol3 [39-41] with fully relaxed atomic structure.

5.1 Effect Due To Single Atom Type Doping

Firstly, the investigation of the effect of single atom doping of N atom (or B atom) on the shifting of the conduction bands (or valence bands) is studied. Doping structures and band structures are listed in Tables 5.1 and 5.2. The illustrated pink atoms, grey atoms and blue atoms indicate B, C, and N atoms, respectively.

Table 5.1 Modeling and Band Structure of 6.25% (B doped)

BGa	BGb	BGc	BGd
Band Gap 0.198eV	Shifting	Shifting	Shifting
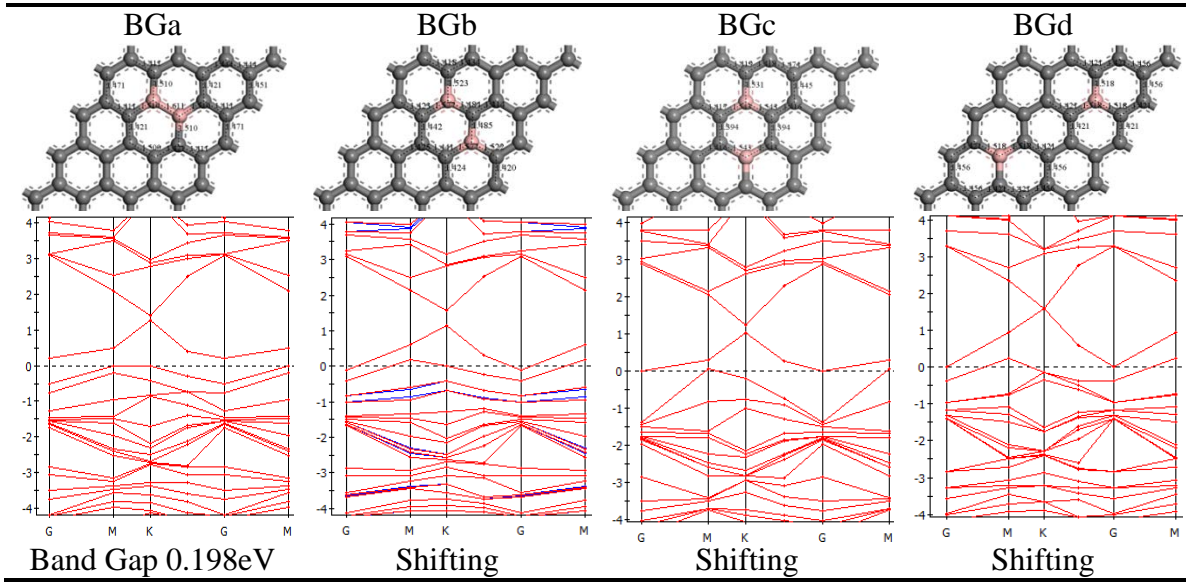
Table 5.2 Modeling and Band Structure of 6.25% (N doped)

NGa	NGb	NGc	NGd
Band Gap 0.146eV	Shifting	Shifting	Shifting
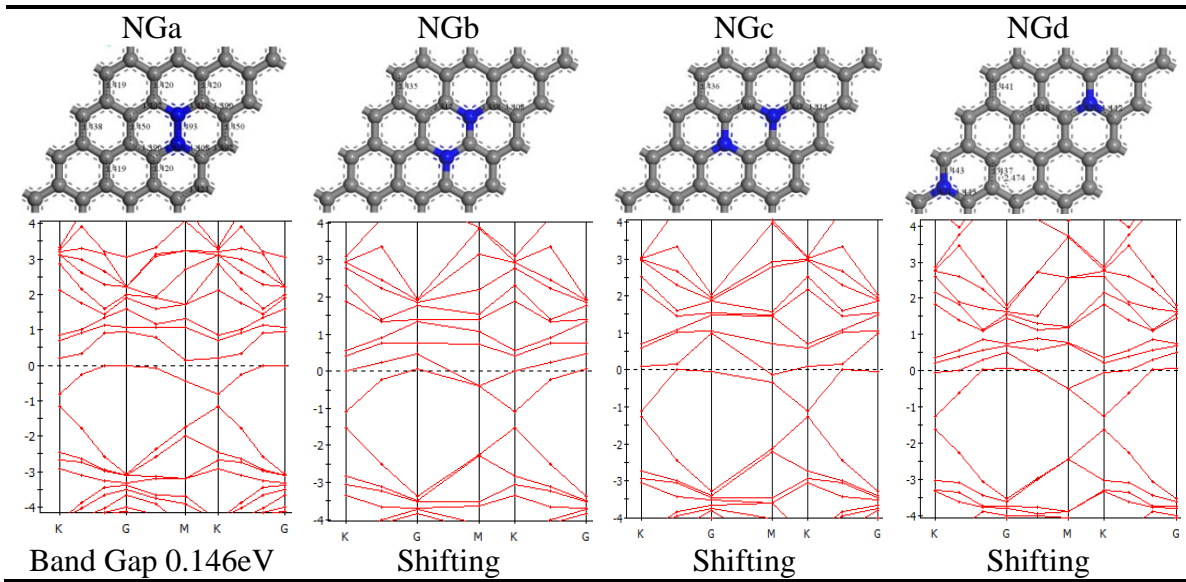
Doping of B atoms causes energy gap above the Fermi level while doping of N atoms causes energy gap below the Fermi level. Adjacent bonded B-B and N-N open a narrow indirect band gap at Fermi level, indicating 0.198eV and 0.146eV, respectively. (See band structure of BGa and NGa in Tables 5.1 and 5.2).

B/N co-doping is expected to open the band gap at the Fermi level. So the co-doping structure was modeled to verify the assumption. Table 5.3 shows the BN co-doping effect on band structure on the same doping sites listed in Tables 5.1 and 5.2.

Table 5.3 Modeling and Band Structure of 6.25% (total B and N codoped)

BNGa	BNGb	BNGc	BNGd
Band Gap 0.384eV	Band Gap 0.110eV	Band Gap 0.39eV	Band Gap 0.217eV
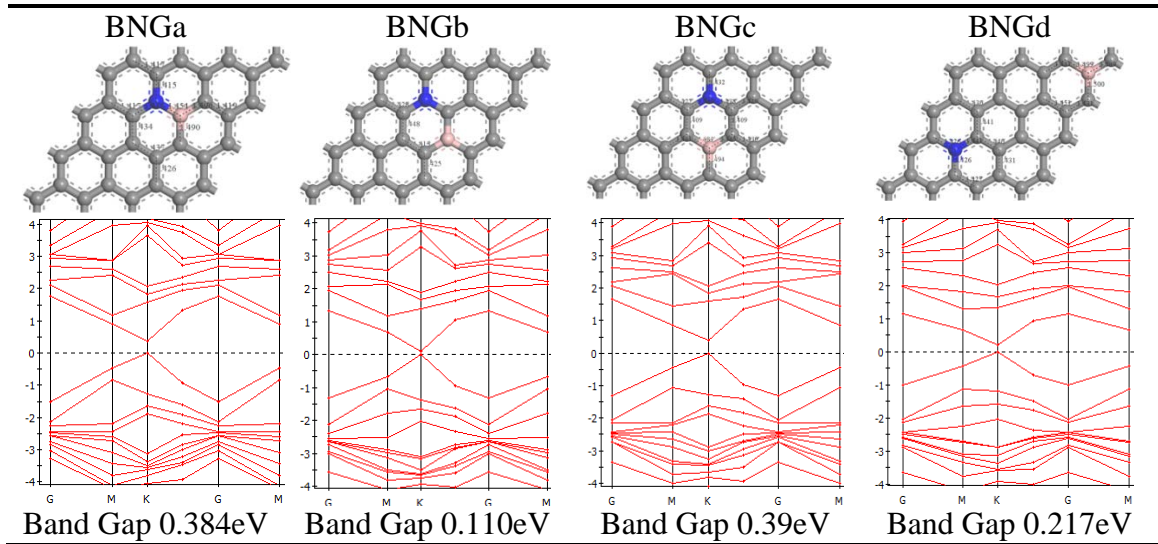
From Table 5.3, we obtain the band gap ranging from 0.110eV to 0.384eV. For adjacent B-N bonded atoms, it opens a wider band gap of 0.384eV compared to 0.198eV resulting from B-B adjacent bond, and also compared to 0.146eV from N-N adjacent bond, at Fermi level.

5.2 CNG (Carbon Nitride Graphene)

In order to further investigate the band gap behavior of N2 Pyridine type N-doped graphene, we created three CNG structures inspired from the literature to investigate their doping effect on graphene [35]. The triangle N2 is differently connected with hexagonal three-coordinated bridging N in CNG1 and CNG2. For CNG3, it has larger void sizes and contains bridged melem units. Only CNG1 and CNG3 open a band gap at the Fermi level of 1.341eV and 0.663eV, respectively.

Table 5.4 Modeling and Band Structure of CNG 57.1% N

(a)CNG1	(b)CNG2	(c)CNG3
Band Gap 1.341eV	Shifting	Band Gap 0.663eV
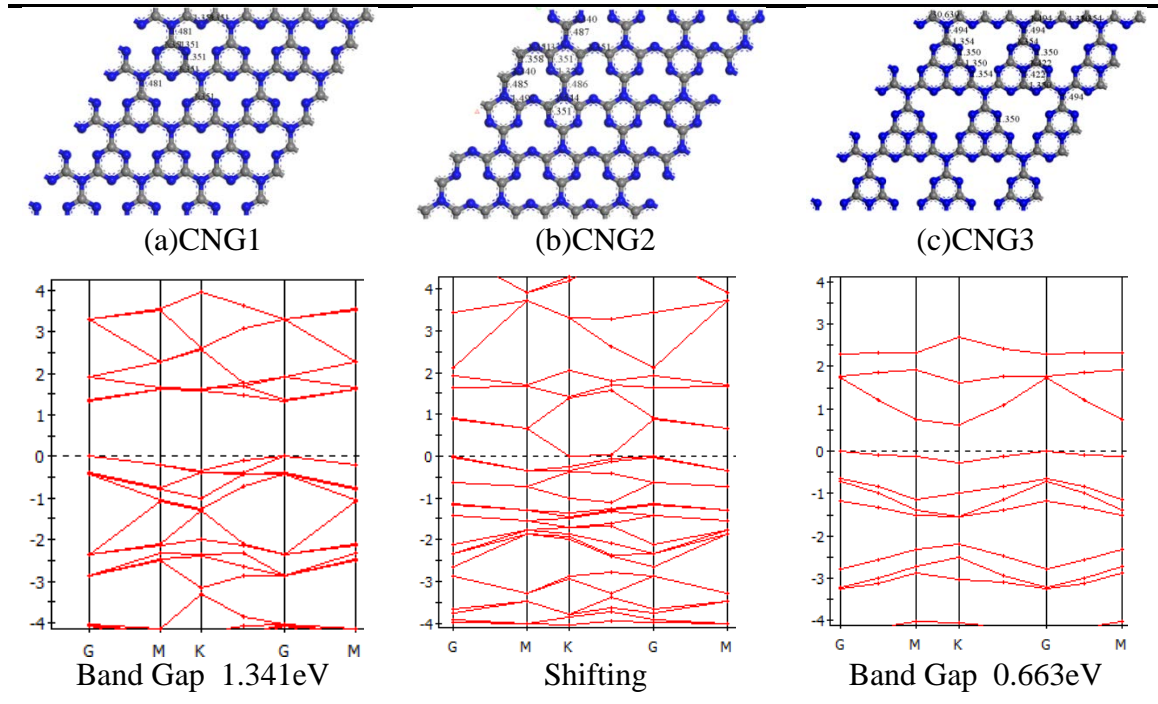
5.3 Co-doping Effect and Isomers

In this section, we will discuss the doping sites, i.e. configuration, of co-doping of B and N atoms. A wider band gap is expected due to increasing doping atoms, along with optimized doping configuration.

(Note: graphene is doped with equal number of boron and nitrogen atoms.)

Table 5.5 Modeling and Band Structure of 25% (total B and N codoped)

BNG1	BNG2	BNG3	BNG4
(a)	(b)	(c)	(d)
DIAGONAL (One B is isolated)	DIAGONAL	B-N DIAGONAL	B-N
Band Gap 1.037eV	Band Gap 1.332eV	Band Gap 1.177eV	Band Gap 0.874eV
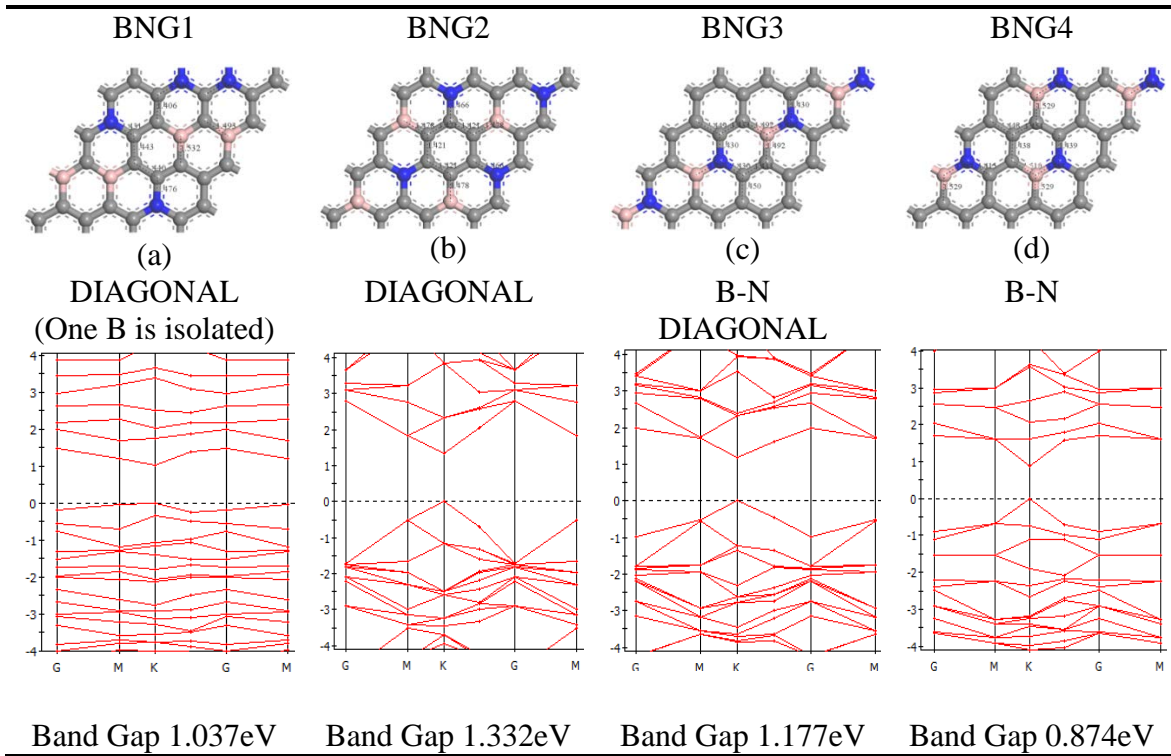
Table 5.6 Modeling and Band Structure of 50 % (total B and N codoped)

BNG5	BNG6	BNG7	BNG8
(e)	(f)	(g)	(h)
B-N ADJACENT& DIAGONAL	B-N, PARRALEL& DIAGONAL	B-N ADJACENT	B-N FULLY
Band Gap 2.026eV	Band Gap 2.283eV	Band Gap 1.454eV	Band Gap 1.019eV
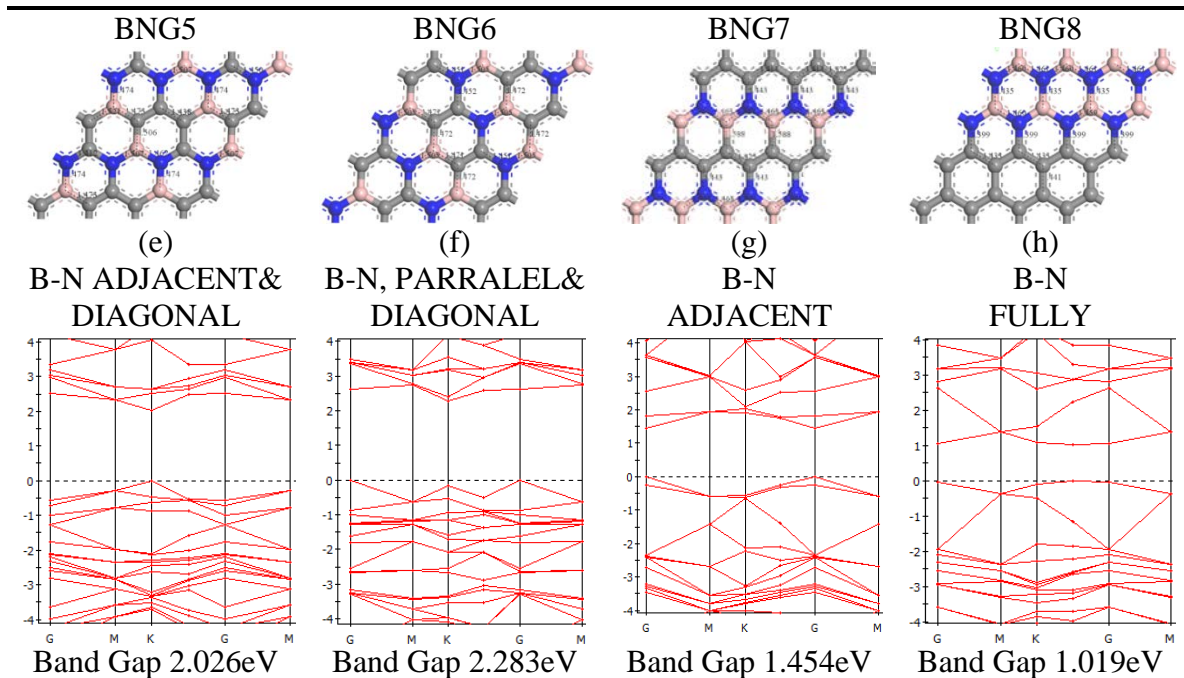
C-B-C bond dominates the band gap behavior, breaks the symmetry of graphene honeycomb symmetry, and hence opens a wide gap value, which can be concluded from all the figures listed in Tables 5.4, 5.5 and 5.6.

B-C-B is the secondary dominant case, which affects the band opening, by comparing Figure (a) and (b) – Table 5.5.

N-C and B-N bond length is similar to C-C bond length which is the least attribute to breaking of symmetry.

By comparing between (c) and (d) – Table 5.5, or between (g) and (h) – Table 5.6, the case of evenly distribution hybridized sp2 bonds, i.e. evenly broken honey-comb-structures, wider band gaps at K-point cannot be ignored.

Comparing (c) - Table 5.5 and (f) - Table 5.6, or (d) - Table 5.5 and (g) - Table 5.6, by introducing more B-N bonds, and meanwhile keeping the same configuration, will definitely increase the band gap.

When C concentration is lower than 50%, B-N bond plays a significant role in breaking of symmetry. Meanwhile, fully and equally occupied comb structure by B and N atoms with the absence of C atoms, inversely decrease the band gap value. The absence of C atoms results in the decrease in C-B bond which is a significant factor that can introduce a wide band gap.

Table 5.7 Modeling and Band Structure of 75% (total B and N codoped)

BNG9	BNG10	BNG11
(i) compared to (g)	(j) compared to (e)	(k) compared to (h)
Band Gap 2.990eV	Band Gap 2.762eV	Band Gap 2.491eV
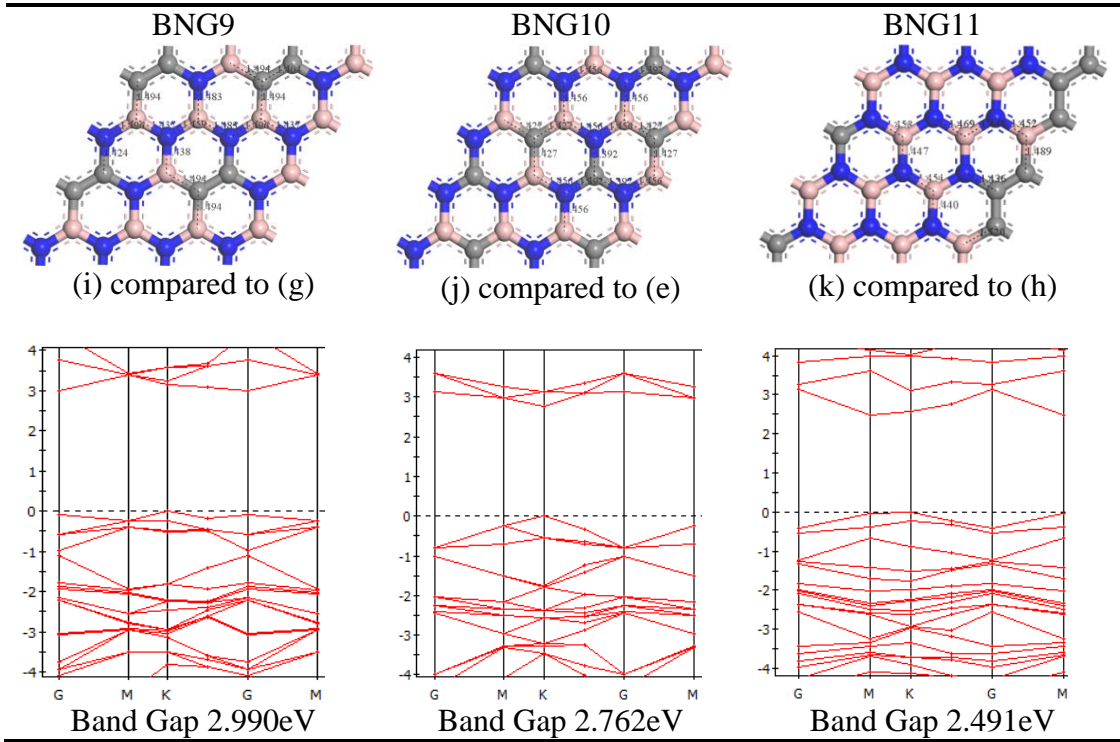
To get a more reliable trend of the variation of the band gap as a function of dopant atoms%, an extensive simulation of various doping concentrations of 18.75%, 37.5% and 62.5% is performed. In Figure 5.1, we can see two ascending lines, which are on the same scale. The red one indicates the maximum optimized value by even distribution of hybridized bonds, and maximization of B-C bonds. The blue line represents the lowest value that was obtained in the simulations. This chart gives an expectation band gap which could be useful to compare with the empirical/experimental results in the near future and provides a reliable data base for band gap design and band gap engineering in graphene-based electronic devices.
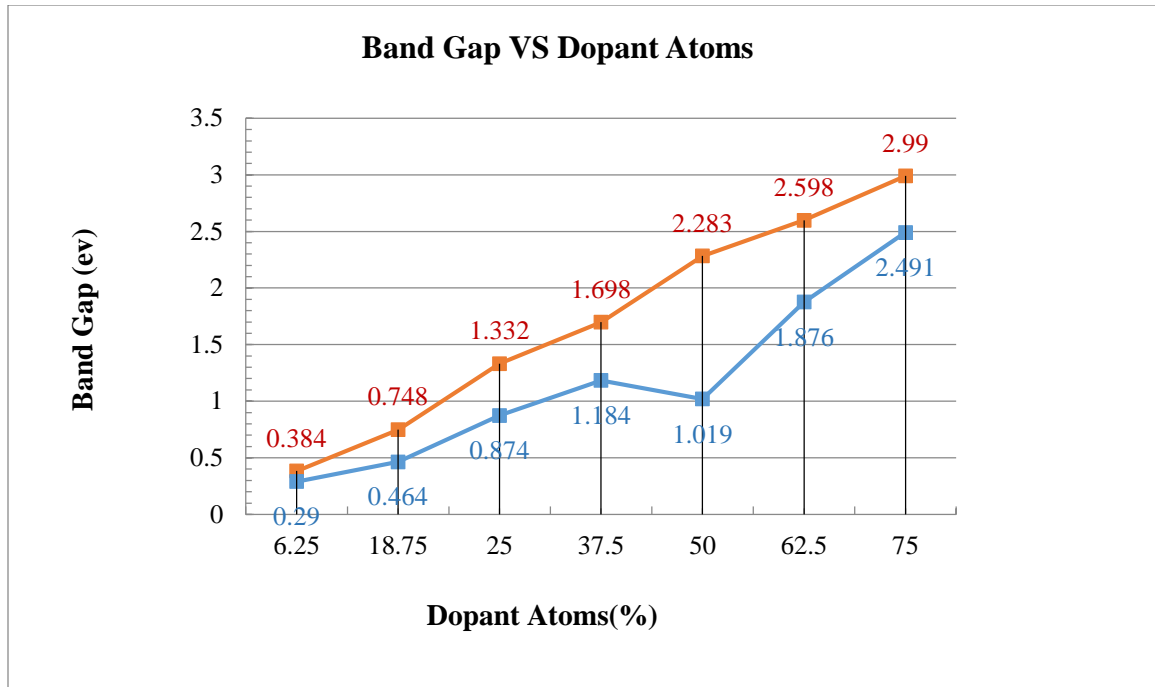
Figure 5.1 Band gap trend as a function of dopant atoms.

To sum up, here is a brief conclusion and suggestion based on the above results:

1. Dopant sites (configuration of C-B, B-N bonds), i.e. isomers will largely affect the gap opening at Fermi level and Dirac point despite the concentration.

2. In lower concentration below 50%, doping sites determine the band gap value; at higher concentration over 50%, the band gap varies slightly, as doping sites are mostly fixed.

3. From the simulation, the largest band gap obtained is 2.99 eV for 75% B-N co-doping.

4. Carbon nitride, chemical composition N_xC_y, can open a band gap at 1.341 and 0.663eV. However, compared to high concentration (over 50%) co-doping, its band gap value is much smaller.

CHAPTER 6

CONCLUSIONS AND RECOMMENDATIONS

Ab-initio calculations based on density functional theory were performed to analyze the physical structure and electronic structure of isomers of B/N codoped graphene sheet and carbon nitride graphene sheet. We observe transition of graphene from semimetal to semiconductor with increasing number of dopants. It has been observed that isomers formed by choosing various doping sites differ in the stability, bond length and band gap introduced, depending on the positioning of the dopant atoms.

Thus, through this detailed analysis, we suggest a theoretical approach to design heteroatom doped graphene with various concentrations of B/N atoms and their isomer configurations. While B or N doping results in band gap at Dirac point with shift in the Fermi Level, B/N co-doping creates the gap at the Fermi level, thus being more efficient and reliable.

Due to their tunable band structure properties, the resulting materials can be used in applications in various sectors, e.g., nano electronics, gas sensing and hydrogen storage. B/N-doped graphene can act as a good electro-catalyst for oxygen reduction reaction (ORR) due to high electron density present on the N atom in BCN heterostructure.

Suggestions for future work:

1. Extend the research to buckled structure other than planar structure studied in this thesis.

2. Explore the stability and formation energy by atomistic scale simulation rather than quantum scale simulation realized in this study using MS.

38

3. Investigate the band gap opening behavior due to additional nanomesh impact and layer impact.

4. Extend the theoretical research to P and Al doping (significant mismatches of heteroatoms) and compare with this study.

REFERENCES

[1] Wallace, P.R. (1947) The band theory of graphite. Physical Review 71(9): 622-634.

[2] Novoselov, K.S., Geim, A.K., Morozov, S.V., Jiang, D., Zhang, Y., Dubonos, S.V., Grigorieva, I.V., Firsov, A.A. (2004) Electric field effect in atomically thin carbon films. Science 306: 666-669.

[3] Novoselov, K.S., Geim, A.K., Morozov, S.V., Jiang, D., Katesnelson, M.I., Grigoreva, V., Dubonos, S.V., Firsov, A.A. (2005) Two-dimensional gas of massless Dirac fermions in graphene. Nature (London) 438: 197-200.

[4] Novoselov, K.S., McCann, E., Morozov, S.V., Falko, V.I., Katsnelson, M.I., Zeitler, U., Jiang, D., Schedin, F., Geim, A.K. (2006) Unconventional quantum Hall effect and Berry's phase of 2p in bilayer graphene. Nature Physics 2: 177-180.

[5] Geim, A.K., Novoselov, K.S. (2007) The rise of graphene. Nature Materials 6: 183-191.

[6] Nair, R.R., Blake, P., Grigorenko, A.N., Novoselov, K.S., Booth, T.J., Stauber, T., Peres, N.M.R., Geim, A.K. (2008) Fine structure constant defines visual transparency of graphene. Science 320: 1308.

[7] Yang, X.B., Liu, G.X., Balandin, A.A., Mohanram, K. (2010) Triple-mode single-transistor graphene amplifier and its applications. ACS Nano 4: 5532-553.

[8] Huang, B., Yan, Q.M., Zhou, G., Wu, J., Gu, B.L., Duan, W.H., Liu, F. (2007) Making a field effect transistor on a single graphene nanoribbon by selective doping. Applied Physics Letter 91: 253122.

[9] Romero, H.E., Joshi, P., Gupta, A.K., Gutierrez, H.R., Cole, M.W., Tadigadapa, S.A., Eklund, P.C. (2009) Adsorption of ammonia on graphene. Nanotechnology 20: 245501.

[10] Bonaccorso, F., Sun, Z., Hasan, T., Ferrari, A.C. (2010) Graphene photonics and optoelectronics. Nature Photonics 4: 611-622.

[11] Wei, D.C., Liu, Y.Q., Wang, Y., Zhang, H.L., Huang, L.P., Yu, G. (2009) Synthesis of N-doped graphene by chemical vapor deposition and its electrical properties. Nano Letters 9(5): 1752-1758.

[12] Castro, A.H., Guinea, F., Peres, N.M.R., Novoselov, K.S., Geim, A.K. (2009) The electronic properties of graphene. Review of Modern Physics 81(1): 109-162.

[13] Kaloni, T.P., Cheng, Y.C., Faccio, R., Schwingenschlogl, U. (2011) Oxidation of monovacancies in graphene by oxygen molecules. Journal of Materials Chemistry 21: 18284-18288.

[14] Kaloni, T.P., Mukherjee, S. (2011) Comparative study of electronic properties of graphite and hexagonal boron nitride (h-BN) using pseudopotential plane wave method. Modern Physics Letter B 22: 1855-1866.

[15] Kaloni, T.P., Upadhyay, K.M., Schwingenschlogl, U. (2011) Induced magnetism in transition metal intercalated graphitic systems. Journal of Materrials Chemistry 21: 18681-1868.

[16] Cheng, Y.C., Kaloni, T.P., Huang, G.S., Schwingenschlogl, U. (2011) Origin of the high p-doping in F intercalated graphene on SiC. Applied Physics Letter 99: 053117.

[17] Wei, X., Wang, M.S., Bando, Y., Golberg, D. (2011) Electron-beam-induced substitutional carbon doping of boron nitride nanosheets, nanoribbons, and nanotubes. ACS Nano 5: 2916-2922.

[18] Liu, H., Liu, Y., Zhu, D. (2011) Chemical doping of graphene. Journal of Materials Chemistry 21(10): 3335-3345.

[19] Xiu, S.L., Zheng, M.M., Zhao, P., Zhang, Y., Liu, H.Y., Li, S.J. (2014). An effective method of tuning conducting properties: First-principles studies on electronic structures of graphene nanomeshes. Carbon 79: 646-653.

[20] Topsakal, M., Cahangirov, S., Ciraci, S. (2010) The response of mechanical and electronic properties of graphene to the elastic strain. Applied Physics Letter 96(9): 091912.

[21] Han, M.Y., Oezyilmaz, B., Zhang, Y., Kim, P. (2007) Energy band gap engineering of graphene nanoribbons. Physical Review Letters 98: 206805.

[22] Zhou, S.Y., Gweon, G.H., Fedorov, A.V., First, P.N., De Heer, W.A., Lee, D.H. (2007) Substrate-induced bandgap opening in epitaxial graphene. Nature Materials 6(10): 770-775.

[23] Giovannetti, G., Khomyakov, P.A., Brocks, G., Kelly, P.J., van den Brink, J. (2007) Substrate-induced band gap in graphene on hexagonal boron nitride: Ab initio density functional calculations. Physical Review B 76: 073103.

[24] Georgakilas, V., Otyepka, M., Bourlinos, A.B., Chandra, V., Kim, N., Kemp, K.C. (2012) Functionalization of Graphene: Covalent and Non-Covalent Approaches, Derivatives and Applications. Chemical Reviews 112(11): 6156-6214.

[25] Zhang, Y., Tang, T.T., Girit, C., Hao, Z., Martin, M.C., Zettl, A. (2009) Direct observation of a widely tunable bandgap in bilayer graphene. Nature 459(7248): 820-823.

[26] Duong, D,L,, Lee, S.M., Chae, S.H., Ta, Q.H., Lee, S.Y., Han, G.H. (2012) Band-gap engineering in chemically conjugated bilayer graphene: Ab initio calculations. Physical Review B 85(20): 205413.

[27] Rakhmanov, A.L., Rozhkov, A.V., Sboychakov, A.O., Nori, F. (2012) Instabilities of the AA-Stacked Graphene Bilayer. Physical Review Letters 109(20): 206801.

[28] Lui, C.H., Li, Z., Mak, K.F., Cappelluti, E., Heinz, T.F. (2011) Observation of an electrically tunable band gap in trilayer graphene. Nature Physics 7(12): 944-947.

[29] Martins, T.B., Miwa, R.H., Da Silva, A.J.R., Fazzio, A. (2007) Electronic and transport properties of boron-doped graphene nanoribbons. Physical Review Letters 98 (19): 196803.

[30] Wang, H., Maiyalagan, T., Wang, X. (2012) Review on recent progress in nitrogen-doped graphene: synthesis, characterization, and its potential applications. ACS Catalysis 2(5): 781-794.

[31] Yu, S., Zheng, W., Wang, C., Jiang, Q. (2010) Nitrogen/Boron doping position dependence of the electronic properties of a triangular graphene. ACS Nano 4 (12): 7619-7629.

[32] Deng, X., Wu, Y., Dai, J., Kang, D., Zhang, D. (2011) Electronic structure tuning and band gap opening of graphene by hole/electron codoping. Physics Letters A 375(44): 3890-3894.

[33] Fan, X., Shen, Z., Liu, A.Q., Kuo, J.L. (2012) Band gap opening of graphene by doping small boron nitride domains. Nanoscale 4: 2157-2165.

[34] Rani, P., Jindal, V. K. (2014). Stability and electronic properties of isomers of B/N co-doped graphene. Applied Nanoscience 4(8): 989-996.

[35] Ci, L., Song, L., Jin, C., Jariwala, D., Wu, D., Li, Y., Srivastava, A., Wang, Z.F., Storr, K., Balicas, L., Liu, F., Ajayan, P.M. (2010)Atomic layers of hybridized boron nitride and graphene domains. Nature Materials 9 (5): 430-435.

[36] Wei, X.L., Wen, X., Xu, L.C., Peng, X.Y., Liu, L.M. (2014) Significant interplay effect of silicon dopants on electronic properties in graphene. Physics Letters A 378(26-27): 1841-1844.

[37] Denis, P.A. (2010) Band gap opening of monolayer and bilayer graphene doped with aluminum, silicon, phosphorus, and sulfur. Chemical Physics Letters 492(4-6): 251-257.

[38] Uday, N.M. (2014) Chemically modified/ doped carbon nanotubes & graphene for optimized nanostructures & nanodevices. Advanced Materials 26: 40-67.

[39] Delley, B. (1996) Fast Calculation of Electrostatics in Crystals and Large Molecules. Journal of Physical Chemistry 100: 6107.

[40] Auckenthaler, A., Blum, V., Bungartz, H.J., Huckle, T., Johanni, R., Kramer, L., Lang, B., Lederer, H., Willems, P.R. (2011) Parallel eigenvalue solution: Parallel solution of partial symmetric eigenvalue problems from electronic structure calculations. Parallel Computing 37: 783.

[41] Giovannetti, G., Khomyakov, P.A., Brocks, G., Kelly, P.J., van den Brink, J. (2007) Substrate-induced band gap in graphene on hexagonal boron nitride: Ab initio density functional calculations. Physical Review B 76(7): 073103.